Experimental and theoretical investigations on interfacial temperature jumps during evaporation

V.K. Badam [a,*], V. Kumar [a], F. Durst [a], K. Danov [b]

[a] *Institute of Fluid Mechanics (LSTM), Friedrich-Alexander-Universität Erlangen-Nürnberg, Cauerstrasse 4, D-91058 Erlangen, Germany*
[b] *Laboratory of Chemical Physics and Engineering, University of Sofia, 1 J. Boucher Avenue, 1126 Sofia, Bulgaria*

Abstract

Experimental results are summarized on investigations of positive temperature jumps at water–vapor interfaces during steady-state evaporation under low-pressure. Steady-state evaporation of water experiments were carried out to measure the interfacial properties and to obtain the evaporation rate. The interfacial vapor temperature close to the interface was always found to be higher than the interfacial liquid temperature. To study the influence of the vapor side thermal boundary conditions on the temperature jump, the evaporation chamber was heated with the help of a heating wire mesh which was mounted in the vapor side plane above the evaporating free surface. It was astounding to the authors to find that the temperature jump at the liquid–vapor interface increases linearly with the heat flux from the vapor side. The maximum temperature jump across the water–vapor interface was measured as 15.68 °C in the presence of vapor phase heating. Still higher temperature jump values can be achieved by applying higher vapor side heat fluxes close to the water–vapor interface. It was attempted to explain these unique experimental results using existing theories of evaporation. Kinetic theory of gases (KTG) predicts the temperature jumps, but the magnitude is 10–20 times smaller than the experimentally obtained temperature jumps. The linearized statistical rate theory yields the evaporation mass flux expression which is same as the KTG expression with evaporation and condensation coefficients of unity. Only non-equilibrium thermodynamics using phenomenological equations appear to predict the magnitude of the temperature jump measured in the experimental study. However, more theoretical work needs to be done to fully understand the new experimental findings reported here.
© 2007 Elsevier Inc. All rights reserved.

Keywords: Evaporation; Temperature jump; Kinetic theory; Non-equilibrium thermodynamics

1. Introduction and objectives

Evaporation and condensation processes are of great importance for a wide range of physico-chemical technologies, meteorological and environmental applications. Evaporation of water at free surfaces has been the subject of investigations by various researchers in the past decades owing to its wide technical applications. Both experimental and theoretical investigations have been carried out in order to understand the evaporation of a pure liquid from its free surface. The evaporation process starts basically at the liquid–vapor surface depending on its interfacial properties across the free interface.

Thermodynamic considerations play an important role in the analysis of interfacial phenomena associated with evaporation and condensation process. According to classical thermodynamics, when two phases coexist in equilibrium, temperature ($T_1 = T_v$), pressure ($P_1 = P_v = P_{sat}$) and chemical potential ($\mu_l = \mu_v$) are continuous across the phase interface and the evaporation rate is zero. Phase change occurs, such as evaporation or condensation, only under non-equilibrium conditions and the continuity of the above mentioned intensive thermodynamic variables at the interface cannot be ensured. Macroscopic thermodynamic and fluid mechanic treatments of the interface assume a sharp discontinuity in the density, but constant

* Corresponding author. Tel.: +49 9131 8529506; fax: +49 9131 8529503.
E-mail address: vbadam@lstm.uni-erlangen.de (V.K. Badam).

Nomenclature

A_i	cross sectional area of surface, m^2
h_l	specific enthalpy of liquid, J/kg
h_v	specific enthalpy of vapor, J/kg
$2H$	mean radius of curvature, 1/m
J_i	thermodynamic flux, $-/m^2$ s
k_h	coupling coefficient
K_e	equilibrium molecular exchange rate, kg/m^2 s
l_{qq}^s	diagonal transfer coefficient of vapor heat flux, W/m^2
l_{ww}^s	diagonal transfer coefficient of evaporation flux, $kg\ s/m^4$
l_{qw}^s, l_{wq}^s	non-diagonal transfer coefficients, kg/m^2 s
L_{ij}	phenomenological Onsager coefficients, W K/m^2
M	molecular weight, kg/mol
$\dot{m}$	net mass flux, kg/m^2 s
$\dot{m}_{lv}$	mass flux from liquid to vapor phase, kg/m^2 s
$\dot{m}_{vl}$	mass flux from vapor to liquid phase, kg/m^2 s
$\dot{q}_i$	heat flux, W/m^2
$\dot{q}_l$	liquid side heat flux, W/m^2
$\dot{q}_v$	vapor side heat flux, W/m^2
R	universal gas constant, J/mol K
R_c	radius of curvature, m
P_l^e	equilibrium liquid pressure, Pa
P_v^e	equilibrium vapor pressure, Pa
$P_{sat}(T_l)$	saturated vapor pressure at liquid temperature, Pa
P_l	liquid pressure, Pa
P_v	vapor pressure, Pa
s	specific entropy, J/kg K
Δs_{lv}	change in entropy, J/kg K
S_{CV}	total entropy per unit area, J/m^2 K

$\dot{S}_e$	entropy change flux, W/m^2 K
$\dot{S}_{irr}$	entropy production, W/m^2 K
T	temperature, K
T_l	liquid phase temperature, °C
T_v	vapor phase temperature, °C
U_i	velocity, m/s
U_l	liquid phase velocity, m/s
U_v	vapor phase velocity, m/s
X_i	thermodynamic forces
V	control volume, m^3

Greek symbols

α	temperature jump coefficient, m^2/W
β	temperature jump coefficient, m^2 s/kg
η_{ev}	evaporation coefficient
η_{con}	condensation coefficient
μ_l	chemical potential of liquid, J/K
μ_v	chemical potential of vapor, J/K
ρ	density, kg/m^3
ρ_l	liquid density, kg/m^3
ρ_v	vapor density, kg/m^3
σ	surface tension, N/m
τ_{ij}	shear stress, N/m^2
ϵ	vibration frequency terms, J/kg K

Acronyms

DFT	density functional theory
KTG	kinetic theory of gases
MD	molecular dynamics
NET	non-equilibrium thermodynamics
SRT	statistical rate theory
PVC	poly vinyl chloride

temperature and pressure across the liquid–vapor boundary. Therefore, it is important to investigate and understand the physical mechanism and the direction of the interfacial discontinuity during the evaporation process. Several theoretical approaches have been used to examine the interfacial conditions during evaporation. Classical kinetic theory of gases (KTG) has provided the molecular basis for understanding the evaporation for over a century [1–3]. Ward and Fang [4] proposed statistical rate theory (SRT) as an alternative to KTG for the treatment of evaporation. Non-equilibrium thermodynamics (NET) treatment provided a good insight into evaporation process [5].

The classical papers of Hertz [1] and Knudsen [2] on the evaporation of liquid mercury into vacuum showed that the interfacial process requires treatment from the viewpoint of the kinetic theory of gases (KTG). With the help of KTG, an expression was derived for the net one-dimensional evaporation mass flux across a liquid–vapor interface in terms of interfacial properties [T_l, T_v and $P_{sat}(T_l)$, P_v]. According to the kinetic theory, non-equilib-

rium effects occur in a kinetic layer (called the Knudsen layer) with a thickness of the order of the molecular mean free path. This treatment considers different temperatures in the liquid and vapor phases just across the liquid–vapor interface. This macroscopic temperature difference is so called "temperature jump" across the interface which is one of the driving force for net rate of evaporation. However, the macroscopic jumps across the interface (temperature, pressure and density changes) are continuous in a microscopic sense but might have sharp gradients of temperature, pressure and density across the liquid–vapor interface region in a molecular length scales, respectively.

The measured value of net rate of evaporation was observed to be much smaller in comparison with the evaporation rate that was predicted according to the developed KTG expression [1,2]. Due to deficiency in prediction, condensation coefficient (η_{con}) and evaporation coefficient (η_{ev}) were defined on a molecular level based on the processes of evaporation and condensation which involve a molecule being emitted from a surface or an impinging molecule being

condensed at the surface. Both Hertz [1] and Knudsen [2] calculated from their measurements the value of the evaporation coefficient. They found from their experiments that the value of evaporation coefficient to be much smaller than the theoretically predicted value of unity. Rideal [6] and some time later Alty [7–9] initiated extensive evaporation experiments with water and noticed that the experimentally obtained evaporation coefficient was two to three orders of magnitude smaller than the theoretically considered value. Schrage [3] further looked into the derivations of KTG for evaporation and modified the Hertz–Knudsen theory by including the net macroscopic velocity of vapor, which is not well represented by a stationary Maxwellian distribution, and suggested the equation, known as the Hertz–Knudsen–Schrage [3] or Kucherov–Rikenglaz [10] equation.

Since then, there have been numerous investigations (e.g. [11–22]) in order to determine "a true value of an evaporation coefficient". In many publications, the evaporation coefficient is not distinguished from the condensation coefficient, both of them being used synonymously. Initially, several futile attempts were made to measure the temperature of the free surface accurately. Later, Prüger [11] performed successful measurements by using two fine thermocouples placed above and below the liquid interface. For several years, Hickman [12] argued that the real value of the evaporation coefficient is unity and, owing to surface contamination, the experimentally obtained evaporation coefficient is less than unity. Barnes [22] indicated, by using the data of Alty [7], a significant decrease in the evaporation coefficient when the surface temperature of water was lowered. Mendelson and Yerazunis [17] observed an increase in the value of the evaporation coefficient as the surface temperature increases. Marek and Straub [23] and Eames et al. [24] presented thorough reviews of the evaporation and condensation coefficients of water which were determined experimentally by various researchers over the past few decades. They reported that the values of evaporation coefficient deduced from different measurements were scattered over four orders of magnitude in the literature [23]. Various arguments can be found in the literature for the significant differences between experimentally obtained and theoretically predicted evaporation coefficients, such as rapid cooling of the interface, impurities at the surfaces and inaccurate measurements of the temperature across the interface [6,7,9,16]. In recent work by Bond and Struchtrup [25], the evaporation mass flux has been obtained by splitting molecular distribution into half-space integrals, under slow evaporation conditions. They considered the condensation coefficient from the transitional state theory and obtained the coefficient values from the experimental results of Fang and Ward [26]. The mean value of the evaporation coefficient has been taken to be same as the mean condensation coefficient, with an assumption that its variations with pressure and temperature may turn out to be negligible [25].

Ward and co-workers [4,26,27] carried out a series of experiments on the steady-state evaporation of water.

Their experiments were carefully performed utilising pure distilled, de-gasified water in order to avoid any impurities in their steady-state evaporation experiments. The temperatures across the interface were measured with a 25 μm thermocouple to yield spatially well-resolved measurements of the local temperature distribution near the investigated water–vapor interfaces. This smaller thermocouple facilitated to move very much closer to the interface than that of any other previous investigations. The temperature measurement was also cross checked with another thermocouple of 81.3 μm in diameter which was mounted 0.5 mm above the 25 μm thermocouple and found the same and consistent readings with both of the thermocouples at a specific location [27]. The found significant temperature jumps[1] across the interface and the vapor phase temperature close to the interface was always higher than the liquid phase temperature [4,26–28]. It is interesting that they measured temperature discontinuities of up to 7.8 °C across the liquid–vapor interface of water with a strong dependence on the vapor side pressure [26].

Ward and Fang [4] proposed that the statistical rate theory (SRT) can account for the evaporation rate on the basis of measured or known values of temperature discontinuity at the interface. They derived a non-linear expression for the mass flux due to evaporation as a function of the entropy change across the liquid–vapor interface. The entropy change is due to a change in the energy properties of the molecules across the interface. The expression of Ward and Fang [4] for evaporation was obtained by adopting two-layer model considerations, and taking into account the thermodynamic states of liquid and its vapor. It was assumed that the properties of the liquid and vapor phases remain unchanged during the transfer of a certain number of molecules.

Another method of constructing the equations for phase change at the liquid–vapor interface is the non-equilibrium thermodynamics (NET). Bedeaux and Kjelstrup [5] derived expressions for evaporation and heat fluxes based on the entropy production equation from non-equilibrium thermodynamics. The NET linear laws are generally with phenomenological transfer coefficients which need to be calculated from all available experimental results. The authors [5] calculated the transfer coefficients using the experimental results of Ward and co-workers [4,26,27] and in some cases the authors obtain unphysical results (see Tables 2 and 3 in Ref. [5]). The density functional theory (DFT) [29] and molecular dynamics (MD) based simulations [30–33] are emerging as most of the fundamental approaches towards understanding of phase change processes. Rosjorde et al. [34]'s non-equilibrium molecular dynamic simulations showed the steep gradients of temperature, pressure and density close to the interfacial region in

---

[1] The measured temperature jumps should not be confused with the temperature gradients; the gradients of temperature at the interface within a 50 μm distance are calculated to be much smaller than the temperature jumps for such precise evaporation experiments.

a microscopical molecular length scales which are significantly different than that of the gradients in either of the bulk phases. One cannot resolve so steep gradients at the interface experimentally and hence referred macroscopically as jump conditions across the liquid–vapor interface. The MD simulations are not discussed further because it is beyond the scope of present experimental and theoretical work.

1.1. Present work

The work reported in this paper was motivated from the experimental results of Ward and co-workers [4,26,27] in which the temperature jump across the water–vapor interface is up to 7.8 °C [26]. Our experimental and theoretical investigations were carried out to elucidate the physics of evaporating liquid–vapor interfaces. For this purpose, initially a rectangular steel channel was built [35,36] and a few preliminary evaporation experiments were conducted. In these results, the maximum observed temperature discontinuities across the water–vapor interface were considerably smaller than those found in the experiments of Fang and Ward [26]. It is observed that both the material of the channel to hold the water and the geometric design of the evaporating water pool are not suitable to obtain controlled results and to understand the evaporation of liquids. Further, the geometrical influence and heat leaks effect on the temperature jumps during evaporation were discussed in detail by Bond and Struchtrup [25].

Steady-state evaporation of water experiments were carried out in a new poly-vinyl chloride (PVC) rectangular test section, which was built to reduce the magnitude of the heat leaks in the setup. It was aimed to observe temperature jumps across the water–vapor interface due to evaporation under low-pressure and to control or enhance the temperature jumps by subsequent steps. It was found from the preliminary basic experiments and theoretical analysis that the temperature jump at the interface, occurring because of evaporation, is a function of the heat fluxes from the liquid and vapor sides. Based on the analysis, new experimental device was designed with a heating element in the vapor phase to enhance the heat and mass transport at the free surface, accordingly enhances the temperature jumps. The vapor phase heat flux to the interface was controlled using the heating element to study the interfacial properties during steady-state evaporation. From the experimental results obtained with the new design, it was observed that the temperature jumps can be varied considerably by changing the heat flux from the vapor side. Interestingly, Bond and Struchtrup [25] also pointed out the similar feature of linearity between temperature jump and vapor phase heat flux during evaporation based on their theoretical investigations. The experimental results obtained from the steady-state evaporation of water, which were described in Section 2, were used to analyse the existing theories. A review of the description of the evaporation phenomenon using the kinetic theory of gases, statistical

rate theory and non-equilibrium thermodynamics is presented in Section 3 and the theories were delved to establish which theory could best explain the experimental results. The major conclusions are summarized in Section 4.

2. Experimental investigation

The experimental investigations on the properties of the water–vapor interface during the phase change process were carried out to acquire a closer understanding of the theoretical results deduced from KTG, SRT and NET. An experimental setup equipped with heating element was constructed to examine the parameters that influence the temperature discontinuities across the free surface. A series of steady-state evaporation experiments on water–vapor system were carried out by following a rigorous experimental procedure for each measurement. The details of the experimental setup and the measuring techniques together with the final results are presented in this section.

2.1. Experimental Technique

A schematic diagram of the experimental setup for the analysis of the evaporation process is shown in Fig. 1. The equipment is as described by Popov et al. [35] with a modified test section, a heating element and an accurate pressure measurement device. The modified evaporation channel with a rectangular opening was made of PVC (23 mm in length and 8 mm in width at the mouth) to suppress the heat leaks, in place of the earlier stainless steel channel of Popov et al. [35] (Fig. 2). An inlet opening is situated at the centre location of the bottom of rectangular channel to inject the liquid. This opening is expanded in such a way that there is negligible effect of the inlet velocity of fluid on the free surface. A pressure transducer (CDG361-211 from INFICON) was connected at the top of the Perspex cylindrical chamber to measure the vapor phase pressure of the system along with a mercury manometer as a reference. The temperature of liquid at the inlet throat of the channel was partially controlled by a liquid circulation system connected to a thermostat bath (MGW Lauda RC6) to avoid nucleation of vapor bubbles along the liquid line.

Distilled, de-ionized and nano-filtered water (ROTISOLV HPLC gradient grade water from Carl Roth GmbH, with a resistivity of 18.0 MΩ cm) was directly introduced into a glass vessel, sealed and de-gassed for 30 min using a pump connected with a liquid nitrogen cold trap. Before starting an experiment, the chamber and syringe were evacuated for 12 h to a pressure of about 10^{-2}–10^{-3} mbar using a turbomolecular pump. The de-gassed water was then filled into the syringe without exposure to air. Once the water surface appeared at the channel brim by purging water from the syringe pump, the liquid in the rectangular-shaped channel was pressurised with nitrogen (about 2.0 bar) to fill water in any possible cavities in the water tube. About 1 h later, the pressure in the chamber was
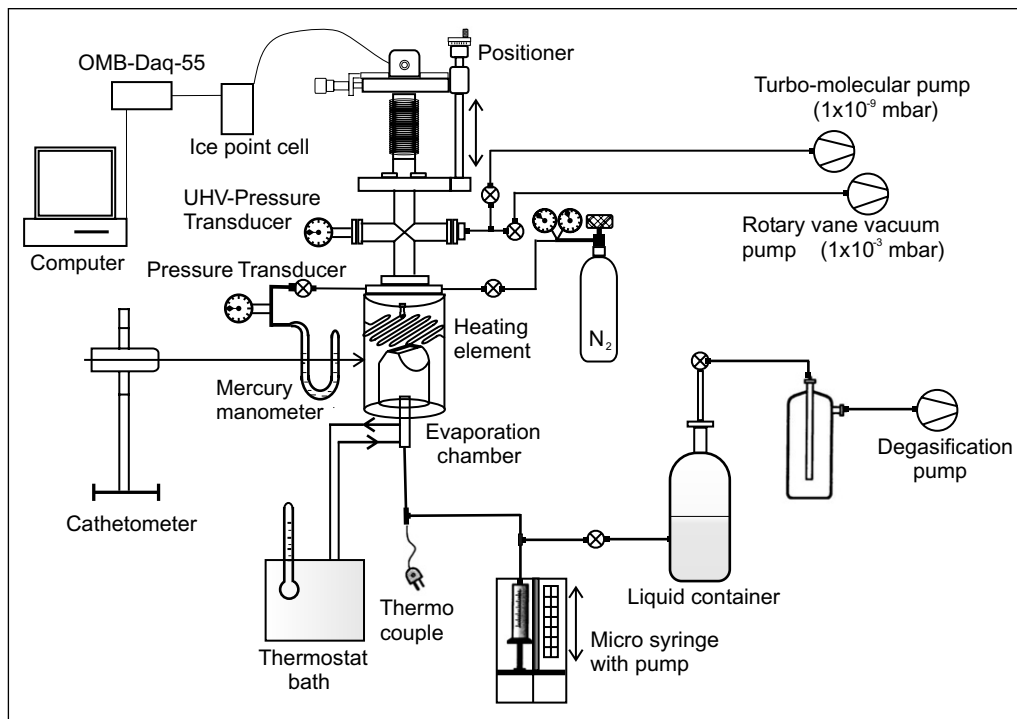
Fig. 1. Schematic diagram of the experimental setup as described by Popov et al. [35] with modified liquid channel and heating element.
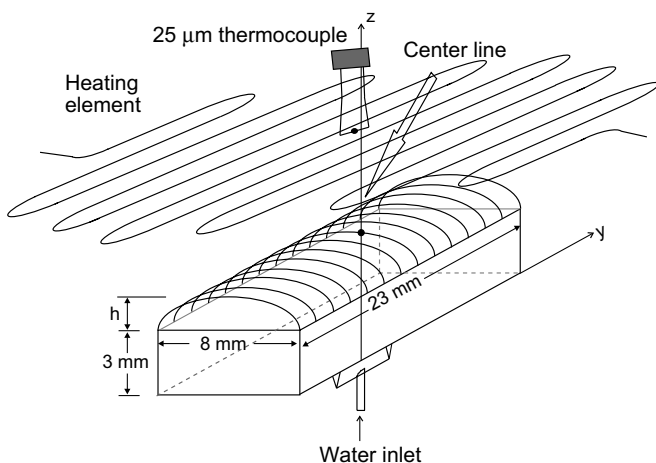

Fig. 2. Modified rectangular trough channel with heating element approximately 3 mm above the free surface.

released and around one-sixth of the water in the syringe was flushed out to remove the upper layer of the liquid in which nitrogen can dissolve. If the nitrogen is present in the liquid even after the flushing of upper liquid, then the nitrogen gas will come out from the liquid surface in the form of bubbles and disturb the free surface during the evaporation and hence steady-state evaporation condition cannot be achieved. After removing upper layer of the liquid, the chamber was evacuated with a rotary vane vacuum pump until it was dry. Thereafter, the water was pumped up to the brim of the channel by the syringe pump. In each experiment, the free surface was maintained

approximately 1 mm above the mouth of the rectangular channel so that the water–vapor interface curvature could be approximated as cylindrical at this height from the edge of the channel. The position of the interface was monitored by a cathetometer with an accuracy of $\pm 10\ \mu m$. The pressure in the vapor phase could be controlled to a certain value by opening and closing the valve of the rotary vane vacuum pump.

A steady-state evaporation rate was obtained by adjusting a metering valve connected to the rotary vane pump and by regulating the flow rate of the micro syringe pump. After a constant interface height (less than $\pm 10\ \mu m$ movement) and vapor phase pressure has been achieved, the system was assumed to be operating under steady-state condition. This specific steady-state condition was maintained throughout the experiment. The movable $25\ \mu m$ thermocouple was positioned on the centreline (shown in Fig. 2) of the channel by monitoring through the cathetometer. The temperatures were measured by moving down the $25\ \mu m$ thermocouple in both vapor and liquid phases in a straight line. The distance between two measurement points was $10\ \mu m$ in the vapor phase near the interface and $20\ \mu m$ in the liquid phase. The second measured point inside the liquid phase was taken to be the liquid phase temperature since the $25\ \mu m$ thermocouple bead is not dipped inside the water completely at the first point of the measurement. Therefore, $50\ \mu m$ is the distance between the vapor and the liquid phase temperature measured points. A heating element grid (shown in Fig. 2) was mounted 3 mm above the free surface to supply different temperatures at the vapor side boundary with the help of

a voltage generator. The basic idea of mounting the heating element at the vapor side is to study the influences of the vapor side heat flux on the interfacial temperature discontinuities and hence to understand the evaporation process. The velocity of the vapor is always in the positive z-direction, hence the heat transfer from the heating element to the free surface takes place only by thermal diffusion. The heat distributed from the heating element to the liquid–vapor interface was assumed to be homogeneous in the present steady-state evaporation experiments. The thermocouple was modified in to U-shape (Fig. 2) in such a way that the ratio of the length of the horizontal section (∼3 mm) to its diameter (25 μm) is sufficiently large so that the thermal conduction along the wires can be neglected [26]. The emissivity of heating element (Constantan material) is ∼0.09 and also the absorptivity of thermocouple bead is less than 1. The order of magnitude analysis indicates that the radiation effect from heating element to the bead of thermocouple is negligible. Hence, the thermocouple reading at any position is accurate and free from the influences of conduction and radiation.

2.2. Measurements and results

Several steady-state evaporation experiments on water were carried out under different operating conditions according to the experimental procedure explained in the previous section. In the first set of experiments, external

heating was not supplied at the vapor side and these experiments are referred as "No heating" experiments from hereafter. After achieving a steady-state condition, by keeping a constant evaporation rate at a particular pressure as explained above, the temperature profiles were measured both in the vapor and in the liquid side at the centreline of the evaporation channel. Initially, a few steady-state evaporation experiments were performed by changing only the vapor pressure of the system. There exists a temperature discontinuity across the water–vapor interface and the temperature at the vapor side of the interface was observed to be higher than that in the liquid side of the interface (Table 1). It is interesting to note that the water remains in liquid state throughout all the experiments even when the pressure of the system is less than 610 Pa (saturated properties of aqueous water below zero degree centigrade are given in [37]). It was observed that the evaporation mass flux increases with decrease in the vapor pressure of the system (Table 1). Moreover, the temperature jump was found to increase with decrease in the vapor pressure of the system. The maximum temperature jump across the water–vapor interface was 3.25 °C at 245 Pa pressure (see Fig. 3). The temperature jumps across the water–vapor interface found by Fang and Ward [26] from their experiments in conical funnel were much larger (up to 8 °C) than those in the present experimental studies which were performed in a rectangular opening channel. It was found by Bond and Struchtrup [25] that larger temperature jumps can be

Table 1

Summary of the steady-state evaporation experiments where thermal conditions were measured at the centreline of the channel

P_v (Pa)	$\dot{m} \times 10^4$ (kg/m² s)	T_1 (°C)	T_v (°C)	$(T_v - T_1)$ (°C)	$\dot{q}_1$ (W/m²)	$\dot{q}_v$ (W/m²)	$(T_v - T_1)$ (°C) KTG	$l_{qq} \times 10^{-4}$ (J/m² s) k_h		$l_{ww} \times 10^8$ (kg²/J m² s) k_h	
								0	0.18	0	0.18
No heating											
561.0	4.70	−1.10	0.73	1.83	546.26	−88.56	0.06	1.33	1.05	162	15.7
490.0	4.92	−2.96	−0.93	2.03	563.81	−94.10	0.08	1.26	1.03	171	14.8
389.1	5.49	−6.02	−3.76	2.27	641.95	−103.69	0.10	1.23	0.66	58.7	12.6
336.5	5.79	−7.90	−5.29	2.60	684.45	−106.03	0.12	1.09	0.41	37.7	10.5
292.4	6.15	−9.61	−6.83	2.78	709.86	−112.01	0.15	1.07	0.16	23.4	8.96
245.3	6.59	−11.67	−8.42	3.25	689.93	−117.14	0.18	0.95	0.03	17.9	7.60
Heating at 30 °C											
736.0	5.78	2.65	6.64	3.99	584.82	−231.45	0.15	1.62	1.62	3610	9.93
569.5	6.07	−0.91	2.93	3.84	659.86	−211.24	0.17	1.52	1.49	546	10.5
483.0	6.36	−3.18	1.04	4.22	685.49	−209.04	0.20	1.36	1.34	833	10.0
391.2	6.87	−6.02	−1.26	4.76	766.51	−221.68	0.26	1.27	1.19	202	9.20
295.2	7.37	−9.51	−4.01	5.50	811.50	−217.71	0.33	1.06	0.74	31.3	6.91
240.3	7.68	−11.85	−6.09	5.76	958.10	−236.99	0.43	1.10	0.62	17.8	5.87
Heating at 40 °C											
736.0	6.71	2.65	7.97	5.33	673.66	−304.84	0.20	1.61	1.60	2860	8.67
567.0	7.16	−0.97	4.82	5.79	698.46	−313.40	0.27	1.50	1.49	642	8.34
485.0	7.34	−3.12	3.02	6.14	785.40	−313.96	0.31	1.41	1.40	713	8.02
392.3	7.80	−5.95	0.57	6.52	781.51	−320.00	0.39	1.34	1.26	123	7.56
288.5	8.32	−9.80	−2.22	7.59	919.74	−327.19	0.53	1.17	0.96	34.9	6.04
236.6	8.53	−12.18	−4.00	8.18	943.22	−335.47	0.66	1.10	0.89	30.0	5.61

The temperature jump predicted from KTG [Eq. (3)] and the interfacial transfer coefficients for water resulted from non-equilibrium thermodynamic relations [Eqs. (22) and (23)] are presented.
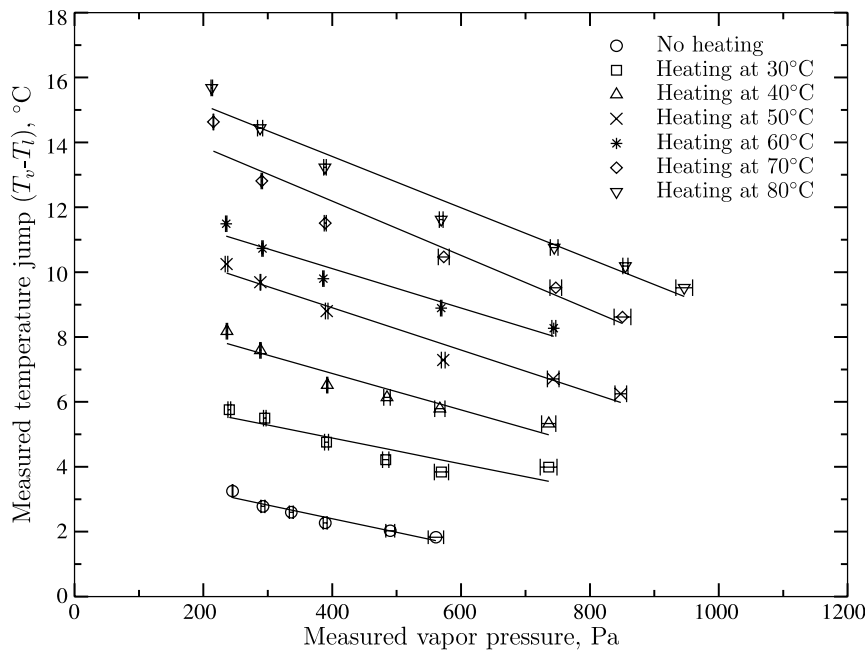
Fig. 3. Measured temperature jump as a function of vapor pressure with different boundary conditions at the vapor side, indicating an increase in the temperature jumps with increase in vapor side heat flux.

observed in spherical geometry, as compared to the planar settings. The amount of liquid phase heat flux and the evaporation flux of water were similar in the present experiments and experiments done by Fang and Ward [26]. It was noticed that the vapor phase heat flux was much higher in Fang's data (133–202 W/m^2) compared with the present results under the similar evaporation conditions (see No heating results in Table 1). This analysis suggests that the $\dot{q}_v$ might influence the temperature jumps across the free surface significantly. Therefore, second set of experiments were conducted by controlling the vapor phase heat fluxes.

In the second set of experiments, the temperature of the heating element was kept initially at 30 °C by applying a constant current and voltage to increase the heat flux from the vapor side. The net evaporation mass flux also increases with respect to the first set of evaporation experiments (without heating case). Under this heating condition, the vapor pressure of the system was varied to observe the influence of vapor pressure on the temperature jump across the evaporating interface. It can be seen from the Table 1 that the maximum temperature jump has increased from 3.25 to 5.76 °C at approximately the same pressure. The temperature of the heating element was increased in a regular steps until 80 °C and a series of experiments were carried out by varying the vapor pressure in each case. The measurements obtained by various thermal boundaries are presented in Tables 1 and 2. The liquid and vapor side heat fluxes were computed from the temperature profiles and thermal conductivities, respectively.

The variation in temperature jumps with the change in vapor pressure and the change in vapor side thermal boundary conditions are presented in Fig. 3 for all experiments. The experimental results indicates that the temper-

ature jump increases predominantly with increase in the vapor side heat flux (vapor side boundary temperature) and also increases with the decrease in vapor pressure of the evaporation system. The temperature jumps can be seen in the experiments even when the vapor pressure of the system is more than 610 Pa (see Tables 1 and 2, more than 10 experiments were above triple point of water). This suggests that the temperature jump phenomena is not due to meta-stable state of water. Only thing is these temperature jumps are significant under low vapor pressure condition compared with the evaporation at higher vapor pressure condition. However, the temperature jump across the interface depends strongly on the vapor side heat flux compared with that of the vapor pressure of the system. The temperature jumps across the water–vapor interface were measured to be as high as 15.68 °C at 213 Pa pressure with increase in the vapor side heat flux for the case of heating at 80 °C (Fig. 4). A typical temperature profile in the water–vapor system is shown in Fig. 4. The liquid side temperature profile is linear, which indicates that thermal conduction is the major mode of energy transport towards the free surface. In order to understand the major contribution of the vapor side heat flux on the temperature discontinuity, the temperature profiles are presented in Fig. 5 at around constant pressure. The temperature discontinuity varies linearly from 2.83 to 11.61 °C with increase in the vapor side heat flux under similar vapor pressure conditions. The phase change processes such as evaporation and condensation are strongly non-equilibrium processes and they indeed inherited with discontinuities (pressure, temperature, entropy, free energy, etc.) at the free surface. In general, it is possible to bring an evaporation process far from the equilibrium state by varying the heat and mass

Table 2
Summary of the steady-state evaporation experiments where thermal conditions were measured at the centerline of the channel

P_v (Pa)	$\dot{m} \times 10^4$ (kg/m² s)	T_1 (°C)	T_v (°C)	$(T_v - T_1)$ (°C)	$\dot{q}_l$ (W/m²)	$\dot{q}_v$ (W/m²)	$(T_v - T_1)$ (°C) KTG	$l_{qq} \times 10^{-4}$ (J/m² s) k_h		$l_{ww} \times 10^8$ (kg²/J m² s) k_h	
								0	0.18	0	0.18
Heating at 50 °C											
847.9	7.66	4.66	10.91	6.25	828.23	−396.63	0.24	1.80	1.77	318	8.33
743.0	7.81	2.79	9.50	6.71	793.81	−396.79	0.27	1.67	1.65	609	7.98
572.4	8.36	−0.92	6.37	7.29	771.91	−417.34	0.36	–	–	–	–
391.4	9.04	−6.03	2.77	8.80	893.47	−411.50	0.51	1.29	1.28	534	6.88
288.5	9.70	−9.82	−0.12	9.69	942.55	−416.22	0.68	1.17	1.02	43.5	5.82
236.0	10.1	−12.21	−1.97	10.25	992.83	−421.29	0.84	1.11	0.95	36.3	5.54
Heating at 60 °C											
866.0	8.10	5.04	12.90	7.86	1138.86	−472.47	0.28	1.72	1.63	86.4	6.68
743.9	8.67	2.80	11.07	8.27	1016.58	−478.56	0.33	1.65	1.64	972	7.27
569.2	9.25	−0.92	7.96	8.89	993.98	−485.88	0.43	1.54	1.53	1370	7.16
386.3	9.86	−5.97	3.83	9.80	1073.50	−490.23	0.62	1.39	1.23	42.7	5.90
291.7	10.5	−9.41	1.33	10.73	1182.54	−500.89	0.81	1.28	1.03	21.9	5.06
235.5	10.8	−12.04	−0.54	11.49	1208.74	−499.86	0.99	1.19	0.96	22.3	4.91
Heating at 70 °C											
966.8	8.82	6.62	10.72	4.10	1255.64	−569.64	0.30	3.95	3.57	83.4	12.7
850.5	9.22	4.75	13.37	8.62	1182.30	−552.41	0.33	1.84	1.77	139	7.15
747.0	9.58	2.86	12.38	9.52	1174.38	−551.72	0.38	1.65	1.65	1633	7.03
573.1	10.2	−0.87	9.60	10.47	1053.56	−571.84	0.50	–	–	–	–
389.2	10.9	−5.94	5.56	11.51	1123.64	−567.60	0.72	1.37	1.28	66.1	5.89
290.7	11.3	−9.58	3.23	12.81	1201.03	−574.88	0.95	1.24	1.08	31.4	5.02
215.6	11.8	−12.99	1.63	14.63	1226.83	−582.59	1.26	1.09	0.91	21.6	4.35
Heating at 80 °C											
1076.8	9.28	8.11	17.82	9.71	1277.74	−591.05	0.28	1.77	1.74	223	6.63
946.3	10.0	6.43	15.95	9.52	1391.01	−637.26	0.34	1.94	1.77	47.7	6.45
855.1	9.87	4.71	14.90	10.19	1270.42	−628.52	0.38	–	–	–	–
744.5	10.6	2.92	13.68	10.76	1307.06	−642.74	0.44	1.71	1.64	103	6.49
569.2	10.9	−0.77	10.84	11.61	1202.59	−655.14	0.58	1.60	1.52	82.0	6.07
388.7	11.6	−5.46	7.77	13.23	1232.48	−647.87	0.79	1.38	1.13	18.7	4.57
288.1	11.9	−9.76	4.69	14.44	1138.66	−650.56	1.10	1.25	1.14	39.9	4.92
213.0	12.3	−13.42	2.27	15.68	1198.74	−623.28	1.41	1.09	1.02	53.2	4.81

The temperature jump predicted from KTG [Eq. (3)] and the interfacial transfer coefficients for water resulted from non-equilibrium thermodynamic relations [Eqs. (22) and (23)] are presented. Dashes indicate a non-physical value of the coefficients since the measured P_v is slightly higher than P_{sat} for evaporation and therefore not computed.

fluxes along the free surface to obtain higher temperature discontinuities. In principle, the sign of the temperature discontinuity can be reversed based on the second law of thermodynamics [38], but this may or may not be achievable experimentally.

3. Summary of theoretical analysis

In this section, the results obtained from the steady-state evaporation of water experiments are used to verify various existing theories such as the kinetic theory of gases, statistical rate theory and non-equilibrium thermodynamics. Further, the evaporation theories are explored to establish which theory can best explain the experimental results.

3.1. Kinetic theory of gases (KTG)

Ever since the pioneering contributions of Hertz [1], and Knudsen [2], the kinetic theory of gases has been widely employed to understand the evaporation of liquids. According to Hertz [1], and Knudsen [2], the molecules are released, or evaporated, $\dot{m}_{lv}$, from the liquid surface of the Knudsen layer according to a half-range Maxwellian distribution function, and depends on the liquid temperature T_1 and the saturation pressure $P_{sat}(T_1)$. On the other hand, molecules impinge from the vapor space on to liquid surface, $\dot{m}_{vl}$, and in a similar way depends on the vapor temperature T_v and the vapor pressure P_v at the vapor boundary of Knudsen layer. It is to be noted that the bulk vapor velocity was assumed to be zero in this derivation. After including the evaporation coefficient, η_{ev} and condensation coefficients, η_{con}, the net mass flux, $\dot{m}$, can therefore be expressed as $\dot{m} = \eta_{ev}\dot{m}_{lv} - \eta_{con}\dot{m}_{vl}$, which results in the Hertz–Knudsen equation:

$$\dot{m} = \sqrt{\frac{M}{2\pi R}}\left[\eta_{ev}\frac{P_{sat}(T_1)}{\sqrt{T_1}} - \eta_{con}\frac{P_v}{\sqrt{T_v}}\right]. \tag{1}$$
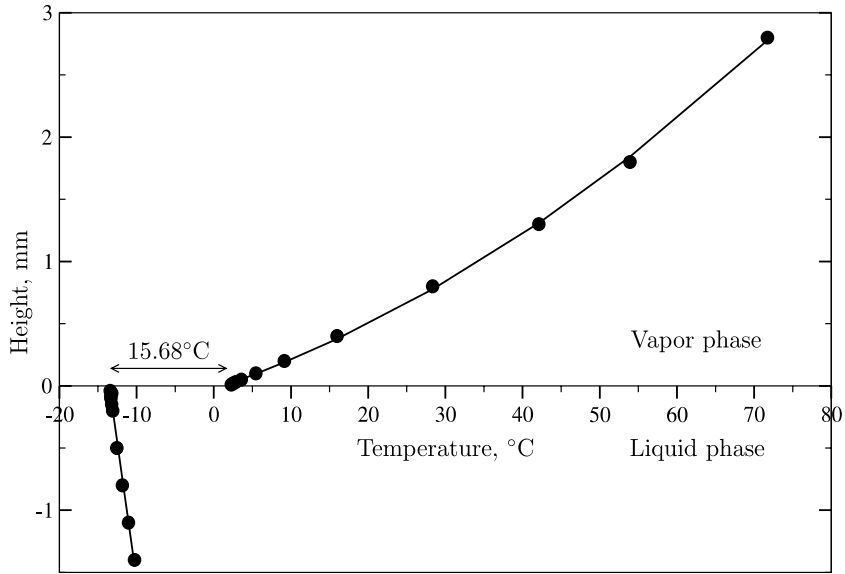
Fig. 4. Liquid and vapor side temperature profiles at 213 Pa pressure for the case where the heating element temperature was maintained at 80 °C. The temperature discontinuity across the interface is 15.68 °C under this evaporation condition.
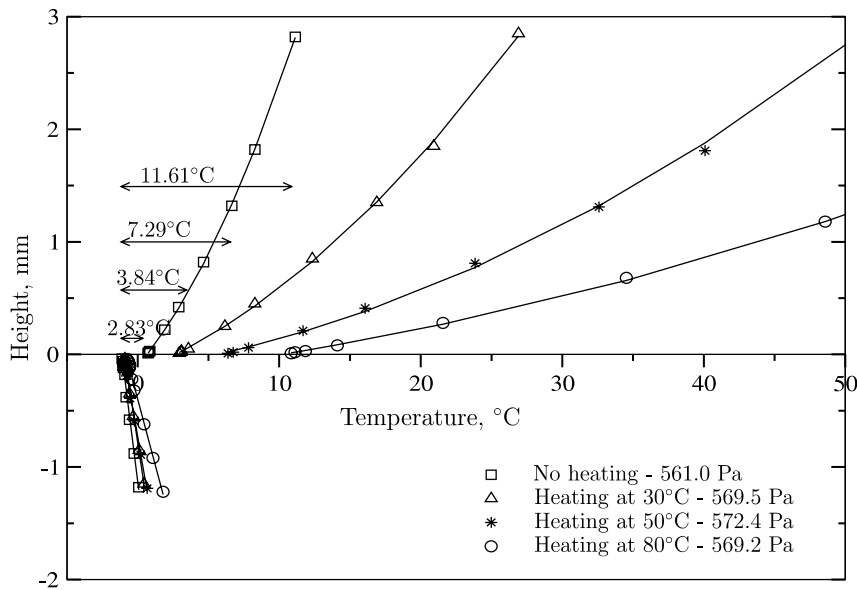

Fig. 5. Liquid and vapor side temperature profiles at around 570 Pa pressure with different heating conditions at the vapor side.

Nevertheless, as already stressed in the Introduction, the theory does not provide consistent results when applied to evaporation experiments and the reasons for this suggested in the literature are not satisfactory [1,2,6–9]. Perhaps the experiments were not commensurate with the assumptions made by the theory. Schrage [3] further corrected the Hertz–Knudsen relation [Eq. (1)] by including the bulk velocity of the vapor in the Maxwellian distribution function and suggested the equation which is known as Hertz–Knudsen–Schrage [3,23] or Kucherov–Rikenglaz equation [10]. After considering $\eta_{ev} = \eta_{con}$ [23], the Hertz–Knudsen–Schrage relation can be simplified to

$$\dot{m} = \frac{2\eta_{ev}}{2 - \eta_{ev}} \sqrt{\frac{M}{2\pi R}} \left[\frac{P_{sat}(T_1)}{\sqrt{T_1}} - \frac{P_v}{\sqrt{T_v}} \right]. \tag{2}$$

The evaporation coefficients are calculated for the present steady-state evaporation of water experiments using Eq. (2). The evaporation coefficients of water obtained for the present steady-state evaporation experiments are significantly scattered, as shown in Fig. 6. Fig. 6 indicates that the evaporation coefficient cannot be defined as a property of the liquid interface. It should be mentioned here that the ±13 Pa accuracy in measuring vapor pressure contributes to some extent to the scatter of the evaporation coefficient.
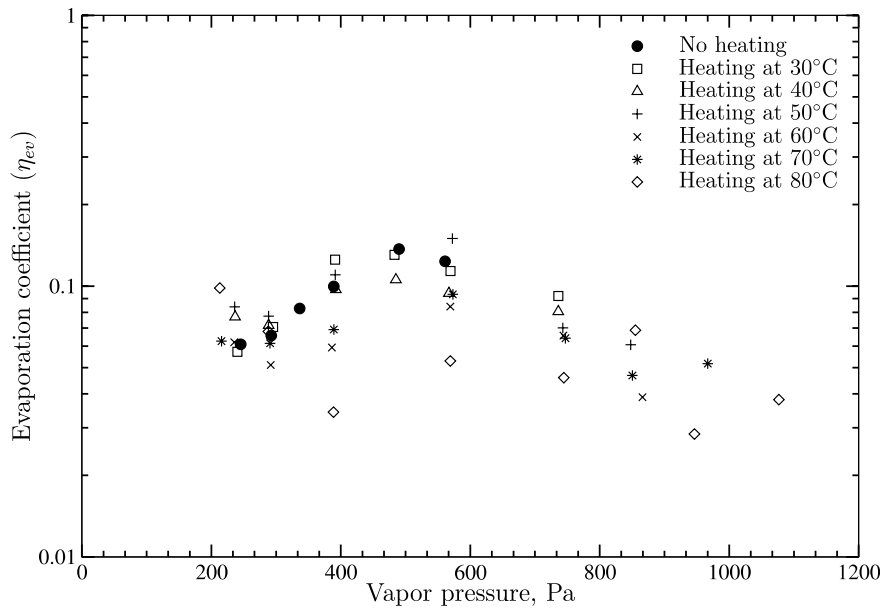
Fig. 6. Variation in magnitude of evaporation coefficient (η_{ev}) of water computed from Eq. (2) for present experiments with different vapor side boundary conditions.

However, for the same saturation pressure, the experimental values of this coefficient are scattered owing to the vapor side boundary conditions (see Fig. 6). This indicates that in reality η_{ev} is a complex function of liquid and vapor temperature, heat fluxes, etc. Hence a constant value of the evaporation coefficient may not be used to predict the evaporation rate. It might be required to correlate η_{ev} in terms of $P_{sat}(T_1)$, which is a controlling parameter at the liquid side and T_v, which indicates the magnitude of non-equivalence. Moreover, η_{ev} and η_{con} were defined [23] in a different way and hence should not be used synonymously. Further, Bond and Struchtrup [25] showed that the condensation probability of individual molecules strongly affects the expression for η_{ev} and η_{con}.

It was pointed out by Barrett and Clement [39] that Schrage's equation for evaporation flux does not conserve momentum and energy. The evaporation rate is driven by the amount of heat supplied to the interface, hence heat and mass flow should be considered to provide a proper theory [25]. Schrage [3] derived Eq. (2) by considering only the thermodynamic states of a liquid and its vapor. Furthermore, the existing theory yielding the Hertz–Knudsen–Schrage equation was started on the basis of the assumption that between the liquid and vapor phases there exists a thin layer, the so-called Knudsen layer. It was claimed that the Knudsen layer remains in equilibrium with both phases. The transport of heat across the Knudsen layer was not taken into account in the considerations of evaporation. It is known that there exists an interface resistance to mass transfer during evaporation which is associated with heat transfer and irreversibilities at any liquid–vapor interface, e.g. see Ishii [40]. However, the kinetic theory model provided in Eq. (2) does not reflect these influences.

By adopting the KTG and irreversible thermodynamics together, Cipolla et al. [41] and Pao [42] derived expressions for the macroscopic jump conditions for temperature and pressure for the case of low evaporation rates with jump coefficients which are functions of temperature and pressure. Cipolla et al. used an approximation method to evaluate the jump coefficient values. Bedeaux et al. [43] referred the KTG expressions of Cipolla et al. [41] and evaluated the various constants of macroscopic jump expressions. The temperature jump expression after evaluation of the jump coefficients (α, β) is

$$\frac{T_v - T_1}{T_1} = -\alpha \dot{q}_v - \beta \dot{m},$$

$$\alpha = 1.03 \sqrt{\frac{M}{2RT_1}} \frac{1}{P_{sat}} \quad \beta = 0.45 \sqrt{\frac{M}{2RT_1}} \frac{R}{M} \frac{T_1}{P_{sat}} \quad (3)$$

The calculated temperature discontinuities at the free surface from Eq. (3) for the present steady-state evaporation experiments are presented in Tables 1 and 2. The theoretically estimated temperature jumps from KTG are 10–20 times smaller than the experimentally observed values. However, it is interesting that the sign of the temperature jump predicted by kinetic theory is the same as that in experiments. Therefore, the statement that "in the case of evaporation the kinetic theory predicts a negative temperature jump at the liquid–vapor interface" presented in many publications [4,5,26,43–46] is not correct.

3.2. Statistical rate theory (SRT)

The SRT is based on the transition probability concept in quantum mechanics and makes use of the Boltzmann definition of entropy to introduce a thermodynamic

description of an evaporating system. The SRT predicts an irreversible evolution to a state that corresponds to the maximum number of quantum mechanical states, which can be far from the states at total equilibrium of the system. The SRT has been applied to various physical rate phenomena, e.g. gas adsorption, thermal desorption, crystal growth from solutions and membrane transport (see, e.g. Ward and co-workers [47–49]). Applying SRT to evaporation, Ward and Fang [4] derived an expression for the evaporation mass flux in terms of thermodynamic variables:

$$\dot{m} = 2K_e \sinh\left(\frac{M}{R}\Delta s_{lv}\right), \tag{4}$$

where K_e is the equilibrium molecular exchange rate between liquid and vapor and Δs_{lv} is the entropy change associated with the transfer of molecules between liquid and vapor contiguous phases. The thermodynamic functions K_e and Δs_{lv} depend explicitly on the physiochemical properties of the system. In the absence of net evaporation mass flux, the K_e can be expressed in terms of equilibrium liquid pressure P_l^e, surface tension σ and mean radius of curvature $2H$ for curved interface as

$$K_e = \sqrt{\frac{M}{2\pi RT_1}}(P_l^e - 2H\sigma). \tag{5}$$

The SRT approach was implemented in the literature [4,26,27,44] for evaporation and used to predict the vapor pressure of the system since the vapor pressure at the free surface cannot be measured very accurately due to the experimental limitations. The predicted value of the vapor pressure is always very close to the magnitude of the saturated pressure at the liquid phase temperature [$P_{sat}(T_1) - P_v$ predicted $\leqslant 10$ Pa]. This magnitude is lower than the accuracy of the measured vapor pressure of the system (± 13.3 Pa). It can be inferred that the SRT predicts the pressure well for the cases which are not too far from equilibrium. This may be because the SRT approach utilised the local equilibrium values to determine the change in entropy due to change of phase of a molecule [4]. In addition, the molecular exchange rates for a unidirectional rate of evaporation and condensation were assumed to be equal to the magnitude of the equilibrium molecular exchange rate.

The free energies of liquid and vapor were assumed to be equal and according to Ward and Fang [4,44] the equilibrium vapor pressure in Eq. (5) can be expressed as

$$P_v^e = P_l^e - 2H\sigma = P_{sat}(T_1) \exp\left[\frac{MP_{sat}(T_1)}{R\rho_1 T_1} - \frac{MP_l^e}{R\rho_1 T_1}\right]. \tag{6}$$

The dimensionless terms in the exponential function of the above equation are fairly small for evaporation experiments at low-pressure. Consequently, Eq. (6) can be linearized and the linear term obtained is substituted in Eq. (5) to give a simplified expression for K_e:

$$K_e \approx \sqrt{\frac{M}{2\pi RT_1}}P_{sat}(T_1)\left(1 + \frac{2H\sigma M}{R\rho_1 T_1}\right)$$
$$\approx \sqrt{\frac{M}{2\pi RT_1}}P_{sat}(T_1). \tag{7}$$

In Eq. (7), the influence of capillary pressure can be ignored for most of the realistic evaporation cases. It is interesting that the equilibrium molecular exchange rate K_e practically coincides with the vaporization from an interface, $\dot{m}_{lv}$, estimated from KTG [first part of Eq. (1)]. The entropy difference Δs_{lv} appearing in Eq. (4) is a function of the temperatures, chemical potentials and enthalpies of the liquid and vapor contiguous phases and can be given by a simplified expression [4]:

$$\Delta s_{lv} = \frac{1}{\rho_1 T_1}[P_v + 2H\sigma - P_{sat}(T_1)] + \frac{4R}{M}\left(1 - \frac{T_v}{T_1}\right)$$
$$+ \frac{R}{M}\ln\left[\left(\frac{T_v}{T_1}\right)^4 \frac{P_{sat}(T_1)}{P_v}\right] + \epsilon, \tag{8}$$

where ϵ represents the vibration frequency terms, which are much smaller than the other terms in Eq. (8), and can be ignored in the process of evaluating the entropy difference Δs_{lv}. The ratios T_v/T_1 and $P_{sat}(T_1)/P_v$ are close to unity, hence the logarithmic term in Eq. (8) can be linearized and the expression for the net mass flux [Eq. (4)] is transformed to

$$\dot{m} \approx 2K_e \frac{M}{R}\Delta s_{lv}$$
$$\approx 2\sqrt{\frac{M}{2\pi RT_1}}P_{sat}(T_1)$$
$$\times \left[\underbrace{\frac{M}{RT_1\rho_1}(P_v - P_{sat}(T_1))}_{I} + \underbrace{\frac{P_{sat}(T_1)}{P_v} - 1}_{II} + \underbrace{\frac{2MH\sigma}{R\rho_1 T_1}}_{III} - \underbrace{2\left(\frac{T_v}{T_1} - 1\right)^2}_{IV}\right]. \tag{9}$$

From Eq. (9), it follows that the capillary pressure term for concave surfaces, III, and the temperature difference term, IV, lead to very small changes in the evaporation mass flux. Hence, in the case of slow evaporation, the linear form of Eq. (9) is

$$\dot{m} \approx 2\sqrt{\frac{M}{2\pi RT_1}}[P_{sat}(T_1) - P_v]. \tag{10}$$

The linear form of the SRT expression for net mass flux is similar to the KTG expression for net mass flux due to evaporation with $\eta_{ev} = \eta_{con} = 1$ [see Eq. (2)]. Experimental observations in the literature indicate that η_{ev} and η_{con} cannot be unity in KTG and also do not conserve momentum and energy. Hence the expression from SRT treatment do not describe the present steady-state evaporation experimental data. In addition, the SRT did not take the transport of heat energy from liquid and vapor phases at the free surface into account [25]. Furthermore, the temperature jumps near the liquid–vapor interface in the phase

change process are not explained by the SRT since there is no expression for the temperature jump.

3.3. Conservation and phenomenological equations

For steady-state interfacial evaporation condition, the continuity and momentum equations are integrated over an arbitrary one-dimensional control volume which consists of both liquid and vapor phases. The following integral conditions can be obtained:

$$\rho_v U_v = \rho_l U_l = \dot{m} \tag{11}$$

and

$$P_l = P_v + \dot{m}^2 \left(\frac{1}{\rho_v} - \frac{1}{\rho_l} \right). \tag{12}$$

The momentum equation results in an integral condition [Eq. (12)] which represents the mechanical equilibrium at the free surface.

Phase change processes are always accompanied by the transport of heat and therefore the energy equation must be integrated. On integrating the enthalpy equation for the present case, the following integral expression can be derived:

$$\frac{1}{2} \dot{m}^3 \left(\frac{1}{\rho_v^2} - \frac{1}{\rho_l^2} \right) + \dot{m}(h_v - h_l) = \dot{q}_l - \dot{q}_v. \tag{13}$$

Eq. (13) is the well-known Stefan condition for a stationary interface where mass transfer is taking place [28]. Note that the viscous dissipation and surface tension terms are omitted in the above equation. The terms $\dot{q}_l$ and $\dot{q}_v$ are conductive heat fluxes from the liquid and vapor sides normal to the interface, respectively, and the term $(h_v - h_l)$ is the latent heat of vaporization. From the above set of integral equations, it is not possible to estimate theoretically the temperature discontinuity at the interface by solving the above set of conservation equations. In order to define the problem uniquely, a condition for the temperature across the surface is essential. Furthermore, one also needs a rate expression to estimate the evaporative mass flux at the interfaces. In the classical thermodynamics, temperature is assumed to be continuous at the interface where the phase change from liquid to vapor takes place. However, this is not always found in experiments; a temperature jump was clearly observed in the present steady-state evaporation experiments and also in the experiments of Ward and co-workers [4,26–28,35,36,44]. A thermodynamic restriction on the process of evaporation is sought here with the help of the entropy production relationship known from thermodynamics. The entropy equation for a unit volume can be derived as (e.g. see Jou et al. [50])

$$\frac{\partial(\rho s)}{\partial t} + \frac{\partial}{\partial x_i} \left(\rho U_i s + \frac{\dot{q}_i}{T} \right) = \dot{q}_i \frac{\partial}{\partial x_i} \left(\frac{1}{T} \right), \tag{14}$$

where s is the specific entropy and T the local temperature in the volume. The second term on the left-hand side is the entropy current and the right-hand side indicates the entropy production due to irreversibilities. Integrating the entropy equation for steady-state conditions over an arbitrary control volume and employing the Gauss divergence theorem yields

$$\int_A \left(\rho U_i s + \frac{\dot{q}_i}{T} \right) dA_i = \int_v \dot{q}_i \frac{\partial}{\partial x_i} \left(\frac{1}{T} \right) dV. \tag{15}$$

Unlike the left-hand side of Eq. (15), the volume integral on the right-hand side cannot be evaluated, i.e. entropy production cannot be directly determined. However, for a steady-state process, the total entropy of a control volume (S_{CV})

$$\frac{dS_{CV}}{dt} = \frac{dS_e}{dt} + \frac{dS_{irr}}{dt} = \dot{S}_e + \dot{S}_{irr} = 0 \tag{16}$$

does not change with time and can be split into two parts: $\dot{S}_e$ is the entropy flux or rate of entropy change due to the flow of heat and mass and $\dot{S}_{irr}$ is the entropy production within the control volume. If the total entropy of the system remains unchanged, then from Eq. (16) and the second law of thermodynamics:

$$\dot{S}_{irr} = -\dot{S}_e \geqslant 0. \tag{17}$$

Integrating Eq. (14) for steady-state evaporation over a control volume consisting of both liquid and vapor phases and comparing the results with Eq. (17), one obtains an equation for entropy production at the free surface:

$$\dot{S}_{irr} = (\dot{q}_v + \dot{m}h_v) \left(\frac{1}{T_v} - \frac{1}{T_l} \right) + \dot{m} \left(\frac{\mu_l}{T_l} - \frac{\mu_v}{T_v} \right) - \frac{\dot{m}^3}{2T_l} \left(\frac{1}{\rho_v^2} - \frac{1}{\rho_l^2} \right) \geqslant 0. \tag{18}$$

In the above equation the term involving the liquid density can easily be neglected, and moreover, the last term on the right-hand side is very small for the present evaporation experiments and can therefore be neglected in this analysis. Consequently, Eq. (18) can be rewritten as

$$\dot{S}_{irr} = \dot{q}_v \left(\frac{1}{T_v} - \frac{1}{T_l} \right) + \dot{m} \left[h_v \left(\frac{1}{T_v} - \frac{1}{T_l} \right) + \left(\frac{\mu_l}{T_l} - \frac{\mu_v}{T_v} \right) \right] \geqslant 0. \tag{19}$$

From non-equilibrium thermodynamics, the entropy production in an irreversible process can be defined as a sum of all thermodynamic forces multiplied with the respective fluxes, i.e.

$$\dot{S}_{irr} = \sum_i J_i X_i, \tag{20}$$

where J_i is the ith thermodynamic flux and X_i the ith thermodynamic force. According to NET [38], the fluxes are linearly related to the all thermodynamic forces responsible for the fluxes i.e.

$$J_i = \sum_j L_{ij} X_j, \tag{21}$$

where L_{ij} are the phenomenological coefficients of the matrix. Bedeaux and Kjelstrup [5] derived expressions for

evaporation and heat fluxes based on the entropy production equation from non-equilibrium thermodynamics, assuming local equilibrium. The local equilibrium assumption is necessary and moreover the assumption has been validated by Johannessen and Bedeaux [51]. Further, the gas phase was assumed to be ideal and by using appropriate thermodynamic relations, Bedeaux and Kjelstrup [5] expressed the final flux equations without neglecting the cross effects from Eq. (19) as [5,43]

$$\dot{m} = -l_{ww}^s \frac{RT_1}{M} \ln\left[\frac{P_v}{P_{\text{sat}}(T_1)}\right] - l_{wq}^s \frac{T_v - T_1}{T_v}, \tag{22}$$

$$\dot{q}_v = -l_{qw}^s \frac{RT_1}{M} \ln\left[\frac{P_v}{P_{\text{sat}}(T_1)}\right] - l_{qq}^s \frac{T_v - T_1}{T_v}, \tag{23}$$

where l_{qq}^s, l_{qw}^s, l_{wq}^s and l_{ww}^s are the components of the Onsager transfer coefficient matrix. According to the Onsager reciprocal principle, the cross coefficients (l_{wq}^s and l_{qw}^s) must be equal and therefore the coefficient matrix is symmetric. In order to have a positive value of entropy production, the diagonal coefficients of the Onsager matrix must be ≥ 0. Bedeaux and Kjelstrup [5] determined these transfer coefficients from the experimental results of Fang and Ward [26]. A coupling coefficient (k_h) was introduced to find the influence of cross effects, i.e. the interaction between the heat and mass fluxes. The term k_h was defined as ratio of the non-diagonal Onsager transfer coefficient (l_{qw}^s) and the diagonal transfer coefficient (l_{ww}^s) of evaporation flux times the vaporization enthalpy [5]. The contribution from the cross coefficients is assumed to be much smaller than that from the diagonal coefficients of the Onsager transfer coefficient matrix. This approximation is not realistic, but is often made to simplify the problem. Therefore at first, the k_h value was taken as zero[2] and later it was assigned the value 0.18, which was found from the KTG. The transfer coefficients l_{qq}^s and l_{ww}^s calculated from the results of Fang and Ward [26] for water, in the case of both values of k_h (0 and 0.18), were of the order of 10^3 W/m^2 and 10^{-8} kg s/m^4, respectively. The coefficient l_{qq}^s for the experiments of Fang and Ward was found to decrease slightly with increase in vapor pressure.

The transfer coefficients were calculated in a similar way for the present experiments by assuming values of coupling coefficient k_h of 0 and 0.18. The vapor side heat flux is calculated with the help of measured temperature profiles along the centreline. The heat and evaporation fluxes along the centreline are assumed to be equal to the average of these fluxes over the free surface. The transfer coefficient values computed for all experimental conditions are presented in Tables 1 and 2. There are two columns each for l_{qq}^s and l_{ww}^s; the first column was obtained with coupling coefficient $k_h = 0$ and the second with $k_h = 0.18$. Owing to the experimental limitations of measuring the vapor

pressure of the system accurately (± 13.3 Pa), the transfer coefficients are not computed for the experiments in which the vapor pressure of the system is slightly higher than the saturated vapor pressure. For $k_h = 0$, the values of both transfer coefficients are found to be positive, indicating that the cross coefficient terms can be neglected, meaning no coupling between the heat and evaporation mass flux. The magnitude of l_{qq}^s is found to be in the range of 10^4 W/m^2, which is 10 times higher than those obtained by Bedeaux and Kjelstrup [5]. The l_{ww}^s coefficient is found to vary by three orders of magnitude from 10^{-5} to 10^{-8} kg s/m^4 (see Tables 1 and 2). The analysis indicates rather tentative results since the magnitudes of the transfer coefficients vary significantly compared with the analysis of Bedeaux and Kjelstrup [5]. The variation in the magnitude of l_{qq}^s may occur because the present experiments were carried out in a PVC channel in which heat leaks from the channel walls are minimised, hence the evaporation rate is minimised under the same operating conditions compared with the experiments of Fang and Ward, which were performed in a stainless steel funnel. The deviation in the value of l_{ww}^s arises because Eq. (22) is sensitive to inaccurate measurement of the vapor pressure (± 13 Pa) of the system.

Bond and Struchtrup [25] have derived evaporation mass flux from phenomenological theory by considering cross coefficients to be zero. Interestingly, it was pointed out by Bond and Struchtrup [25] that the evaporation mass flux expression of NET is similar to the linearized form of the SRT expression [see Eq. (9)]. Therefore, the Onsager coefficient (l_{ww}^s) is equivalent to $2K_e \frac{M}{R}$ from the SRT equation close to equilibrium conditions. Ward and Fang [4] showed the sensitivity of the SRT evaporation rate expression [Eq. (4)] by making small changes in the independent variables. They found that Eq. (4) cannot be utilised directly to compute the magnitude of the evaporation flux from measured quantities since the accuracy of measured variables is limited by the experimental conditions.

The sensitivity of evaporation flux equation [equation (50) of Ref. [25]] from NET is estimated by including the entropy difference, Δs_{lv}, Eq. (8). The lower magnitude terms, the vibration frequency (ϵ) term and the term with liquid density in the denominator, are ignored for this analysis. The errors in measuring T_1, T_v and the radius of curvature (R_c) are negligible compared with the deviation in vapor pressure (± 13 Pa) of the system, and the total error in the calculated mass flux is given by

$$\frac{\Delta \dot{m}}{\dot{m}} = \frac{1}{\dot{m}} \frac{\partial \dot{m}}{\partial P_v} \Delta P_v + \frac{1}{\dot{m}} \frac{\partial \dot{m}}{\partial T_1} \Delta T_1 + \frac{1}{\dot{m}} \frac{\partial \dot{m}}{\partial T_v} \Delta T_v + \frac{1}{\dot{m}} \frac{\partial \dot{m}}{\partial R_c} \Delta R_c$$

$$\frac{\Delta \dot{m}}{\dot{m}} = -\frac{l_{ww}^s}{\dot{m}} \frac{R}{M} \frac{\Delta P_v}{P_v} + \cdots$$

$$= -\frac{461.4 l_{ww}^s}{\dot{m}} \frac{\Delta P_v}{P_v} = -\frac{461.4}{\Delta s_{\text{lv}}} \frac{\Delta P_v}{P_v}. \tag{24}$$

When Eq. (24) is observed quantitatively by considering the experiment with a high rate of evaporation (Table 2),

---

[2] In the case of zero cross effects, i.e. the off-diagonal coefficients of the Onsager matrix are much smaller than the the diagonal coefficients, then the value of k_h is zero by definition.

it is found that a 5% error ($\pm$13 Pa) in measuring the vapor pressure can give up to a 400% error in computing the evaporation flux. Hence the evaporation flux cannot be computed quantitatively from any of the relations [Eqs. (4) and (22)] owing to the experimental limitations in measuring the vapor pressure of the system. In addition, the measured rate of evaporation is an averaged quantity along the free surface and the local evaporation flux might vary at each point along the free surface. However, it is not possible to measure the local evaporation rate at each point on the free surface experimentally, hence the local and average evaporation fluxes are assumed to be equal. The NET evaporation mass flux without cross coefficients [Eq. (22)] can be used to predict the vapor pressure of the system in a similar way as in the SRT approach [4,26,27,44]. However, the analysis in the Appendix shows that the evaporation flux expression predicts the vapor pressure always approximately equal to the saturated vapor pressure at liquid temperature. It is supported by Table A.1 that even a 100% error in temperature discontinuity or more than 50% error in evaporation flux does not influence the prediction of the vapor pressure.

The crossover force term for the evaporation flux in Eq. (22), the temperature discontinuity across the water–vapor interface $(T_v - T_l)/T_v$ (in which temperatures can be measured within accuracy of $\pm$0.2 K), was plotted against the measured net evaporation flux as shown in Fig. 7. It is not possible to include two driving forces, pressure force and temperature discontinuity, together from Eq. (22) to observe the net evaporation flux due to the two unknown Onsager coefficients. The measured evaporation mass flux is found to be a linear function of temperature discontinuity according to Eq. (22) without including the major driving force, i.e. the pressure force at the liquid–vapor interface [see Fig. 7]. It can be observed that as the vapor pressure of the system increases, the cross coefficient term of Eq. (22) (slope of the curves in Fig. 7) is increasing and at the same time, the magnitude of major driving force is decreasing (intercept of the curves in Fig. 7). Fig. 7 indicates that the magnitude of major driving force (pressure force) is predominant as compared with the thermal force for evaporation mass flux. Equations of the curves in Fig. 7 suggests that $\dot{m}$ is of the order of 10^{-4} kg/m^2 s due to pressure force (intercept) even when the thermal force is zero. The influence of different driving forces on evaporation mechanism can be studied further by conducting similar experiments at different operating conditions. It is still to be elucidated that what fraction of mass flux is driven by pressure difference and by temperature jump.

Based on Eq. (23), the vapor side heat flux ($\dot{q}_v$) was plotted against the driving force (temperature jump) at three different constant pressures as shown in Fig. 8. The results indicate that the temperature jump across the evaporating free surface is a linear function of the applied vapor phase heat flux. The experimental observations agree well with the analysis of Bond and Struchtrup [25] who estimated that the interfacial temperature jump depends on the temperature gradient of the vapor just above the interface. Fig. 8 suggests that the temperature jump depends mainly on the applied vapor phase heat flux and also depends on the vapor pressure of the evaporation system. It can be observed from the Fig. 8 that the major driving force (temperature jump) for vapor phase heat flux relation [see Eq. (23)] is significantly higher than the cross over force. The value of the Onsager coefficient (l_{qq}^s) was evaluated from the plotted results using Eq. (23). It was found to be of the order of 10^4 W/m^2 and is a function of vapor pressure of the system. As the vapor pressure of the system increases,
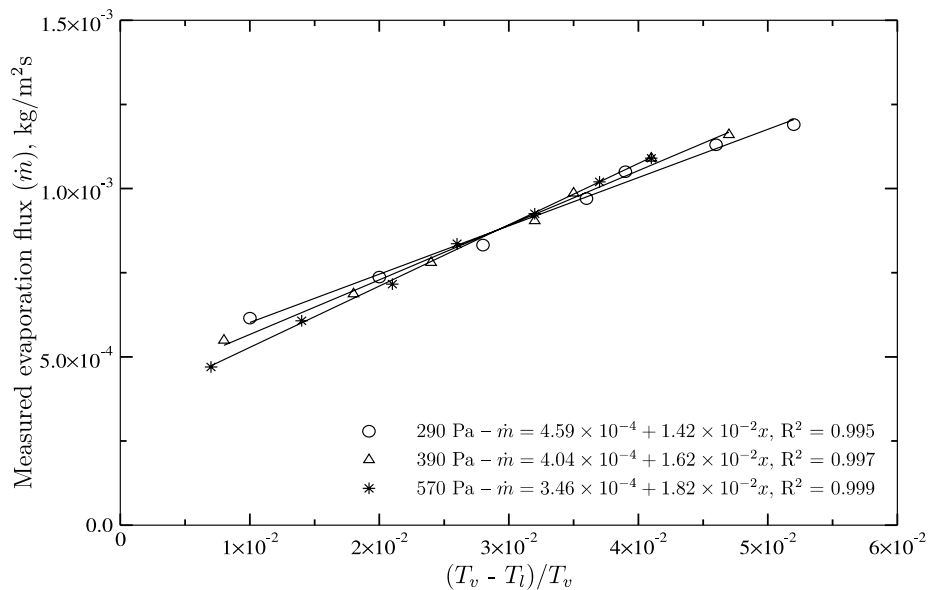

Fig. 7. Measured evaporation flux as a function of driving force in accordance with Eq. (22) by neglecting the diagonal component. The x-represents the driving force, $(T_v - T_l)/T_v$.
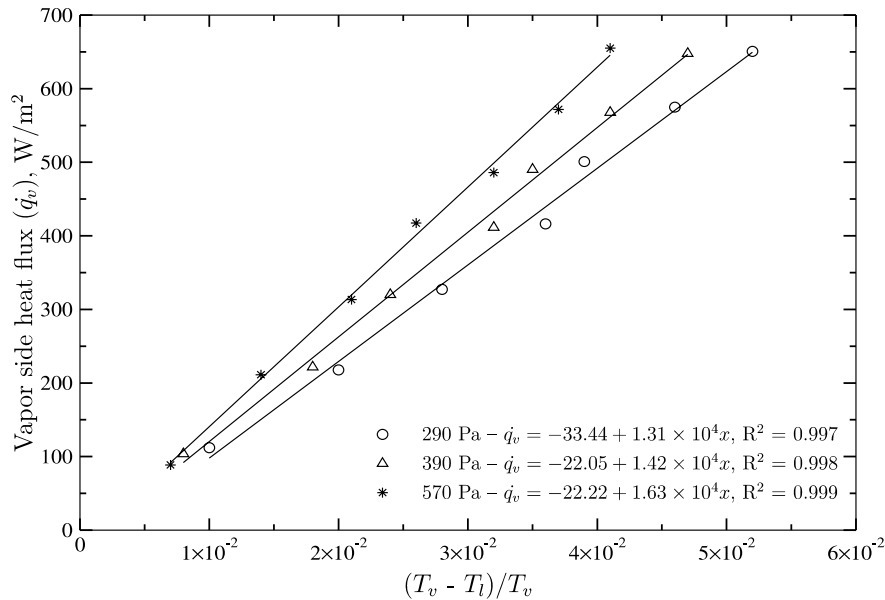
Fig. 8. The vapor side heat flux (computed from the measured temperature profile) as a function of driving force in accordance with Eq. (23) by neglecting the cross coefficient. The x-represents the driving force, $(T_v - T_l)/T_v$.

the Onsager coefficients increase accordingly (Fig. 8). Hence, The NET expression for vapor phase heat flux which was derived by Bedeaux and Kjelstrup [5] seems to predict the behaviour of the evaporation process. The experimental results confirms that the vapor phase heat flux is linear and a strong function of the diagonal component force, i.e. the temperature jump force, and a weak function of the non-diagonal component force, i.e. the pressure jump force across the free surface.

4. Conclusions

The steady-state evaporation of water results have been found to be consistent with previous experimental work at the author's institute [35,36] and the experimental work of Ward and co-workers [4,26–28,44]. The uniqueness of the present experimental setup is to have an external vapor side heat source, which allows one to investigate the influence of vapor side heat flux on the evaporation process. The main features of the steady-state evaporation results under low-pressure conditions are as follows:

- The temperature jump across the liquid–vapor interface has been found during the evaporation process; the vapor phase temperature is always higher than the liquid phase temperature close to liquid–vapor interface at the present slow rate of evaporation experiments.
- The temperature discontinuity at the free surface is a strong function of vapor side heat flux. The temperature discontinuity increases with increase in the vapor side heat flux.
- The temperature discontinuity depends on the vapor pressure of the system. As the vapor pressure decreases, the temperature jump across the liquid–vapor interface increases.

- The maximum temperature jump across the water–vapor interface is shown to be as high as 15.68 °C by implementing strong vapor side heat flux.

A qualitative and quantitative analysis of the KTG, SRT and NET have been presented based on the steady-state evaporation of water experimental results at low-pressures and under the influence of a vapor side heat source. The evaporation coefficient of water from KTG was found to vary significantly in the present experiments from 0.028 to 0.15. However, the smaller values of η_{ev} in the present results compared with the theoretical value of unity might be due to the influence of heat fluxes and temperature jumps across the interface. The temperature jumps at the interface are also predicted with the help KTG and appear to be much smaller than the measured temperature jumps. The SRT expression for net evaporation mass flux was linearized and found that the linearization gives expression similar to the KTG with evaporation coefficients equal to unity. The SRT predicts the vapor pressure of the evaporation system which are always close to the saturation pressure.

Exclusively the non-equilibrium theoretical approach gives the vapor side heat flux expression as a linear function of temperature discontinuity, where otherwise it is not possible to correlate heat fluxes with temperature jumps using KTG or SRT. The expression for the vapor phase heat flux is in good agreement with the experimental results. The magnitude of the phenomenological coefficient of vapor phase heat flux expression is of the order of 10^4 W/m^2 and it is found to vary with the vapor pressure of the system. Once the vapor side heat flux is known, the temperature discontinuity across the liquid–vapor interface can be estimated. The analysis of evaporation mass flux expressions from KTG, SRT and NET suggests that the evaporation mass flux cannot be directly predicted

from the interfacial properties and further investigations are needed to understand the evaporation mechanism.

Acknowledgements

Appendix A

The expression for the evaporation flux from NET was obtained by Bond and Struchtrup (Eq. (50) in Ref. [25]) without considering the cross coefficients. When the entropy difference between the liquid and the vapor in the above relation was taken from a simplified Eq. (8) then

$$\dot{m} = l_{ww}^s \Delta s_{lv}$$

$$= l_{ww}^s \left(\underbrace{\frac{1}{\rho_1 T_1} [P_v + 2H\sigma - P_{sat}(T_1)]}_{I} + \frac{4R}{M}\left(1 - \frac{T_v}{T_1}\right) \right.$$
$$\left. + \frac{R}{M}\ln\left[\left(\frac{T_v}{T_1}\right)^4 \frac{P_{sat}(T_1)}{P_v}\right] + \epsilon \right). \quad (A.1)$$

The first term (I) and the last term (ϵ) on the right-hand side of Eq. (A.1) are much smaller than the other terms and therefore can be neglected. Consequently, the above equation is transformed to

$$\ln\left[\left(\frac{T_v}{T_1}\right)^4 \frac{P_{sat}(T_1)}{P_v}\right] = \frac{\dot{m}}{l_{ww}^s}\frac{M}{R} - 4\left(1 - \frac{T_v}{T_1}\right). \quad (A.2)$$

Eq. (A.2) can be rearranged to yield the vapor pressure:

$$P_v = P_{sat}\left[\left(\frac{T_v}{T_1}\right)^4 \exp\left\{-\frac{\dot{m}}{l_{ww}^s}\frac{M}{R} + 4\left(1 - \frac{T_v}{T_1}\right)\right\}\right]. \quad (A.3)$$

The Onsager coefficient (l_{ww}^s) is equivalent to $2K_e\frac{M}{R}$ of the SRT Eq. (9) and is of the order of 10^{-5} kg s/m^4. Therefore, the first term in the exponent is a small quantity $\left(\frac{\dot{m}}{l_{ww}^s}\frac{M}{R} \approx 10^{-2}\right)$ and can be neglected. The ratio of the absolute temperatures between vapor and liquid is usually close to unity $\left(\frac{T_v}{T_1} \approx 1\right)$. Hence the vapor pressure of the system is expected to be approximately same as the saturated pressure at liquid temperature ($P_v \approx P_{sat}$).

The above analysis is examined quantitatively with the highest rate of evaporation result obtained from the present evaporation experiments (see Table 2). First, the temperature jump is intentionally set to zero, i.e. by bringing the vapor temperature equal to the saturated temperature of the liquid (Table A.1). It is interesting that the predicted vapor pressure from Eq. (A.3) remains close to its satu-

Table A.1
The vapor pressure from Eq. (A.3) is predicted to testify that the value is always close to the saturated vapor pressure at the liquid temperature

	Mass flux ($\dot{m}$)	Measured P_v	P_{sat}	ΔT	Predicted P_v
Actual measurement	1.23×10^{-03}	213.0	217.1	15.68	215.0
Hypothesis one				0	216.6
Hypothesis two	4.70×10^{-04}				215.4

rated vapor pressure even with such a large error in temperature jump as shown in Table A.1. Hence it may be concluded that the predicted pressure is always close to the saturated value irrespective of the magnitude of the temperature discontinuity.

In the next hypothetical case, the mass flux is erroneously set to a value of the lowest evaporation rate, from the present experimental results which is at 561 Pa pressure (see Table 1), by keeping all other conditions constant. It is assumed to calculate the influence of the mass flux on the prediction of the vapor pressure from Eq. (A.3). The predicted vapor pressure value remains unchanged (see Table A.1) since the exponential term of Eq. (A.3) is a small quantity, i.e. equal to zero.

References

[1] H. Hertz, Über die Verdungstung der Flussigkeiten, inbesondere des Quecksilbers, im luftleeren Raume, Ann. Phys. Chem. 17 (1882) 177–200.

[2] M. Knudsen, Die Maximale Verdampfungsgeschwindigkeit des Quecksilbers, Ann. Phys. Chem. 47 (1915) 697–708.

[3] R. Schrage, A Theoretical Study of Interphase Mass Transfer, Columbia University Press, New York, 1953.

[4] C. Ward, G. Fang, Expression for predicting liquid evaporation flux: statistical rate theory approach, Phys. Rev. E 59 (1) (1999) 429–440.

[5] D. Bedeaux, S. Kjelstrup, Transfer coefficients for evaporation, Physica A 270 (1999) 413–426.

[6] E.K. Rideal, On the influence of thin surface films on the evaporation of water, J. Phys. Chem. 38 (1924) 1244–1247.

[7] T. Alty, The reflection of vapor molecules at a liquid surface, Proc. R. Soc. London A 131 (1931) 104–116.

[8] T. Alty, The maximum rate of evaporation of water, Philos. Mag. 15 (96) (1933) 82–103.

[9] T. Alty, C. Mackay, The accommodation coefficient and the evaporation coefficient of water, Proc. R. Soc. London A 149 (1935) 104–116.

[10] R. Kucherov, L. Rikenglaz, The problem of measuring the condensation coefficient, Dok. Akad. Nauk SSSR (Phys. Chem. Sect.) 133 (1960) 735–737.

[11] W. Prüger, Die Verdampfungsgeschwindigkeit der Flüssigkeiten, Zeitschrift für Physik 115 (1940) 202–244.

[12] K. Hickman, Maximum evaporation coefficient of water, Ind. Eng. Chem. 46 (7) (1954) 13–29.

[13] E. Kappler, Eine neue Methode zur Bestimmung von Kondensations-Koeffizie- nten von Wasser, Technical Report 3 (125), Wirtschafts- und Verkehrministeriums Nordrhein-Westfalen, 1955.

[14] N. Fuchs, Evaporation and droplet growth in gaseous media, Pergamon Press, Oxford, 1959.

[15] N. Campbell, A study of turbulent mass transfer at high transfer rates, Ph.D. thesis, Rensselaer Polytechnic Institute, Troy, NY, 1964.

[16] L. Delaney, R. Houston, L. Eagleton, The rate of evaporation of water and ice, Chem. Eng. Sci. 19 (1964) 105–114.

[17] H. Mendelson, S. Yerazunis, Mass transfer at high mass fluxes: Part I. Evaporation at the stagnation point of a cylinder, AIChE J. 11 (5) (1965) 834–840.

[18] H. Cammenga, H. Klinge, B. Rudolph, Untersuchungen über die Verdampfungsgeschwindigkeit von Flüssigkeiten, Fortschrittsberichte über Kolloide und Polymere 55 (1971) 118–123.

[19] J. Maa, Evaporation coefficient of liquids, Ind. Eng. Chem. Fundam. 6 (4) (1967) 504–518.

[20] Y. Finkelstein, A. Tamir, Interfacial heat transfer coefficients of various vapors in direct contact condensation, Chem. Eng. J. 12 (1976) 199–209.

[21] U. Narusawa, G. Springer, Measurements of evaporation rates of water, J. Colloid Interface Sci. 50 (1975) 392–395.

[22] G. Barnes, Insoluble monolayers and the evaporation coefficient of water, J. Colloid Interface Sci. 65 (2) (1978) 567–572.

[23] R. Marek, J. Straub, Analysis of the evaporation coefficient and the condensation coefficient of water, Int. J. Heat Mass Transfer 44 (2001) 39–53.

[24] I. Eames, N. Marr, H. Sabir, The evaporation coefficient of water: a review, Int. J Heat Mass Transfer 40 (12) (1997) 2963–2973.

[25] M. Bond, H. Struchtrup, Mean evaporation and condensation coefficient based on energy dependent condensation probability, Phys. Rev. E 70 (6) (2004) 061605-1–061605-21.

[26] G. Fang, C. Ward, Temperature measured close to the interface of an evaporating liquid, Phys. Rev. E 59 (1) (1999) 417–428.

[27] C. Ward, D. Stanga, Interfacial conditions during evaporation or condensation of water, Phys. Rev. E 64 (1999) 1–9.

[28] C. Ward, F. Duan, Turbulent transition of thermocapillary flow induced by water evaporation, Phys. Rev. E 69 (5) (2004) 056308-1–056308-10.

[29] T. Wadewitz, J. Winkelmann, Application of density functional perturbation theory to pure fluid liquid–vapor interfaces, J. Chem. Phys. 113 (2000) 2448–2455.

[30] M. Matsumoto, Molecular dynamics simulation of interphase transport at liquid surfaces, Fluid Phase Equilibria 125 (1996) 195–203.

[31] S. Kjelstrup, T. Tsuruta, D. Bedeaux, The inverted temperature profile across a vapour/liquid surface analyzed by molecular computer simulations, J. Colloid Interface Sci. 256 (2002) 451–461.

[32] G. Nagayama, T. Tsuruta, A general expression for the condensation coefficient based on transition state theory and molecular dynamics simulation, J. Chem. Phys. 118 (3) (2003) 1392–1399.

[33] J. Xu, S. Kjelstrup, D. Bedeaux, A. Rosjorde, L. Rekvig, Verification of Onsager's reciprocal relations for evaporation and condensation using non-equilibrium molecular dynamics, J. Colloid Interface Sci. 299 (2006) 452–463.

[34] A. Rosjorde, S. Kjelstrup, D. Bedeaux, B. Hafskjold, Non-equilibrium molecular dynamics simulations of steady-state heat and mass transport in condensation. II. Transfer coefficients, J. Colloid Interface Sci. 240 (2001) 355–364.

[35] S. Popov, A. Melling, F. Durst, C. Ward, Apparatus for investigation of evaporation at free liquid–vapor interfaces, Int. J. Heat Mass Transfer 48 (2005) 2299–2309.

[36] F. Duan, V. Badam, F. Durst, C. Ward, Thermo-capillary transport of energy during water evaporation, Phys. Rev. E 72 (2005) 056303-1–056303-11.

[37] R.C. Weast (Ed.), CRC Handbook of Chemistry and Physics, 60th ed., CRC press, 1979–80.

[38] I. Prigogine, Introduction to thermodynamics of irreversible processes, Interscience, New York, 1965.

[39] J. Barrett, C. Clement, Kinetic evaporation and condensation rates and their coefficients, J. Colloid Interface Sci. 150 (2) (1992) 352–365.

[40] M. Ishii, Thermo-fluid Dynamic Theory of Two-phase Flow, Eyrolles, Paris, 1975.

[41] J. Cipolla, H. Lang, S. Loyalka, Kinetic theory of condensation and evaporation. II, J. Chem. Phys. 61 (1) (1974) 69–77.

[42] Y.-P. Pao, Temperature and density jumps in the kinetic theory of gases and vapors, Phys. Fluids 14 (7) (1971) 1340–1346.

[43] D. Bedeaux, L. Hermans, T. Ytrehus, Slow evaporation and condensation, Physica A 169 (1990) 263–280.

[44] C. Ward, G. Fang, Examination of the statistical rate theory expression for liquid evaporation rates, Phys. Rev. E 59 (1999) 441–453.

[45] T. Ytrehus, Theory of gas kinetics in evaporation, in: L. Potter (Ed.), In Rarefied Gas Dynamics, vol. 51, AIAA, New York, 1977, pp. 1197–1212.

[46] T. Ytrehus, Molecular-flow effects in evaporation and condensation at interfaces, Multiphase Sci. Technol. 9 (1997) 205–325.

[47] C. Ward, The rate of gas absorption at a liquid interface, J. Chem. Phys. 67 (1) (1977) 229–235.

[48] J. Elliott, C. Ward, Temperature programmed desorption: a statistical rate theory approach, J. Chem. Phys. 106 (13) (1997) 5677–5684.

[49] M. Dejmek, C. Ward, A statistical rate theory study of interface concentration during crystal growth of dissolution, J. Chem. Phys. 108 (1998) 8698–8704.

[50] D. Jou, J. Casas-Vázquez, G. Lebon, Extended Irreversible Thermodynamics, Springer, Berlin, 1996.

[51] E. Johannessen, D. Bedeaux, The non-equilibrium van der Waals square gradient model. (II). Local equilibrium of the gibbs surface, Physica A 330 (2003) 354–372.